Presented as an invited talk at the 1998 Applied Superconductivity Conference and submitted for publication in *IEEE Transactions on Applied Superconductivity.* SRF 981009-07

Field Emission and Thermal Breakdown in Superconducting Niobium Cavities for Accelerators

J. Knobloch
Laboratory of Nuclear Studies, Cornell University, Ithaca, NY 14853

***Abstract*—Field emission and thermal breakdown are the main mechanisms limiting the accelerating gradient of niobium radio-frequency cavities. Diagnostic tools to study these mechanisms include quality measurements, thermometry, and microscopy. Results presented here demonstrate that micron-size, conducting particles are the source of field emission. Thermal breakdown is caused by a variety of defects such as inclusions, pits, and submillimeter-size particles. Techniques developed to minimize field emission and thermal breakdown include clean-room assembly, high-power processing (to avoid field emission) and the use of high-purity niobium (to avoid thermal breakdown). With these techniques, accelerating gradients of 20–30 MV/m can be achieved in niobium cavities.**

I. Introduction

In particle accelerators, copper radio-frequency (RF) cavities have traditionally been called upon to supply energy to the beam. However, superconductivity offers attractive alternatives because of its low RF losses. This technology has been proven in accelerators such as HERA (DESY, Germany), TJNAF (Newport News, VA), and LEP-II (CERN, Switzerland). The maximum accelerating gradient ($E_{\rm acc}$) of such cavities is determined by the RF critical magnetic field. Niobium cavities for electron–positron accelerators are hence limited to 50 MV/m. However, such high gradients are rarely achieved. Common limiting mechanisms are *electron field emission* (FE) and *thermal breakdown* (TB).

Presently, FE limits cavities to below $E_{\rm acc} \approx 25$ MV/m. In the presence of the high surface-electric field, RF power is lost to electrons that tunnel out of the cavity wall at very localized points. FE scales exponentially with the electric field and is capable of consuming inordinate amounts of power.

TB generally results when a highly resistive defect at the RF surface is the source of a thermal instability that causes the cavity to quench. TB may occur even below the onset of FE.

Extensive cavity research over the last 25 years has lead to the development of sophisticated diagnostic tools, such as temperature mapping and microscopy. As a result, both FE and TB nowadays are well characterized and understood. Based on this information, techniques are being used to reduce the occurrence of cavity defects (or at least minimize their impact), leading to impressive cavity-performance improvements.

II. Diagnostic tools

The diagnostic techniques can be divided into two groups: global methods and local methods. The following list is by no means complete:

A. Global diagnostic techniques

Global techniques measure an average for the entire cavity. They are very useful in identifying the dominant loss mechanism.

1) Cavity quality factor measurement: Standard cavity tests include the measurement of the cavity quality Q_0 as a function of $E_{\rm acc}$ (or the peak surface-electric field $E_{\rm pk}$). The Q_0 is defined as the ratio of the stored energy to the dissipated power times the angular frequency of the cavity mode.[1] In the absence of anomalous losses, the Q_0 is independent of $E_{\rm acc}$.

Measurements of the cavity response to a square input power pulse are used to determine the Q_0 (e.g., [1]).

The Q_0 is very useful, because it measures the sum of *all* losses, and the shape of the Q_0 versus $E_{\rm acc}$ curve can identify the dominant loss mechanism. For example, if the Q_0 drops exponentially at high field, FE is a likely culprit.

2) Current measurements and x-ray detection: FE can be detected with a biased electron-pickup probe in the cavity and an x-ray detector outside the cryostat (for bremsstrahlung x rays). Both are useful for detecting the onset of FE and to measure the emitter strength, provided one FE site dominates the cavity.

B. Local diagnostic techniques

To be able to locate individual defects and emitters, mapping techniques are required. Again, many types have been developed and only a short overview is given.

1) Thermometry: Ultimately, most of the dissipated power heats the cavity wall. Thus, an ideal system for studying all loss mechanisms is an array of temperature sensors on the cavity exterior. Reviews of such systems are given in a number of references (e.g., [2], [3]).

Common to all systems are the temperature sensing elements—usually 100 Ω Allen-Bradley carbon resistors. These thermometers are specially prepared to provide thermal contact to the cavity wall, while shielding them from the liquid He bath. An example is shown in Fig. 1(a).

With a fixed array of thermometers (Fig. 1(b)), temperature maps can be acquired in as little as 0.2 s. Thus,

Manuscript received September 15, 1998. Work supported by the National Science Foundation.

[1]The Q_0 is simply 2π times the number of RF cycles it takes to dissipate an energy equal to that stored in the cavity.

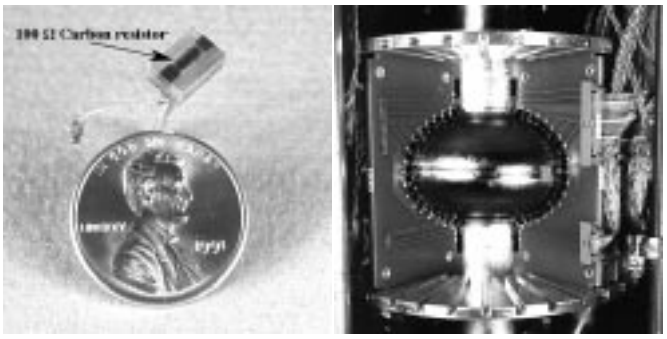

(a) (b)

Fig. 1. (a) A carbon thermometer. (b) Thermometers mounted on a 1.5-GHz cavity.

Fig. 2. SEM used for the examination of 1.5-GHz half cells.

short lived cavity events and the evolution of loss mechanisms with $E_{\rm acc}$ can be studied. State-of-the-art systems can detect temperature rises on the order of 0.1 mK, so that both high- and low-level losses are observable.

2) X-ray detection: Arrays of small scintillators mounted near the cavity surface have been used to study the spatial distribution of x rays [4]. Frequently, x-ray maps are similar to the corresponding temperature maps. However, spurious signals result from x-ray reflections and scattering, complicating the evaluation of the maps. Also, not all losses (e.g., TB) can be observed by x-ray mapping.

3) Light detection: Due to the intense heating of microscopic defects during FE, visible light emission can occur in cavities. A special cavity was developed at Saclay to study the intensity and spectra of field emitters [5].

4) Microscopy: The ability to examine cavity defects in a scanning electron microscope (SEM) and an energy dispersive x-ray system (EDX) is also available. The technique was developed at CERN [6], and then adapted at Cornell for 3-GHz [7] and 1.5-GHz cavities [8] (see Fig. 2). The cavities have to be cut apart cleanly to permit the examination. Despite the cost, the opportunity to examine defects diagnosed by thermometry during RF tests has proven to be a *very* powerful tool. An alternative solution, using a break-apart "mushroom" cavity, was developed at Cornell, whereby the high-electric-field region of its demountable end plate can be examined in an SEM [9]. However, no thermometry data is available for this system.

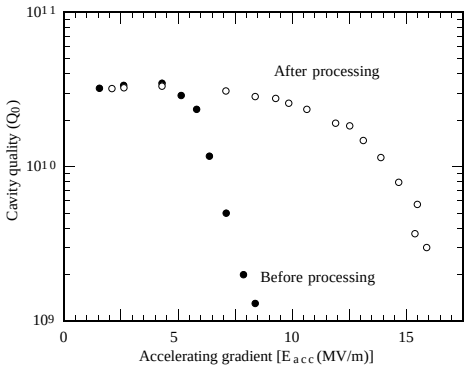

Fig. 3. Q_0 versus $E_{\rm acc}$ curve of a FE-loaded cavity.

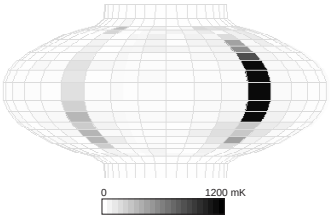

Fig. 4. Temperature map of a 1.5-GHz cavity with two emitters.

III. Field emission

It is known that FE is due to quantum tunneling of electrons from microscopic defects on the RF surface, assisted by the cavity's electric field. Most field emitters occur in the high-electric-field regions near the cavity irises. An in-depth discussion of FE is given in [1], [10].

A. Diagnosing field emission

FE is characterized by an exponential drop of the Q_0 versus $E_{\rm acc}$ curve, usually above $E_{\rm acc} = 5$ MV/m (Fig. 3). At the same time, energetic (0.1–1 MeV) x rays can be detected.

In accelerating the FE charges, the electromagnetic field dissipates power, leading to the declining Q_0. The accelerated current impacts the cavity walls, producing heat (observable by thermometry) and bremsstrahlung x rays. At times, the heating can be so severe that a quench results. Due to the symmetry of the typical accelerating cavity eigenmode, the electron motion is confined to the azimuth of the emitter, yielding the characteristic line heating shown in Fig. 4. By comparing the heating profile with simulated profiles, one can infer the emitter location [1], [8].

Occasionally, an emitter abruptly extinguishes ("processes" or "conditions") and the Q_0 improves (Fig. 3). Based on extensive thermometry, microscopy, and numerical simulations, a model of the processing mechanism has now been developed. It is discussed briefly later.

Similar to FE processing, the abrupt (and irreversible) activation of FE at a threshold field is possible. In some cases the activation can be correlated with the administration/redistribution of gases in the cavity [8], [11].

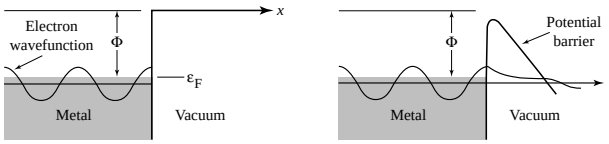

(a) (b)

Fig. 5. Electrostatic potential of the metal–vacuum interface. (a) No electric field applied, (b) with an electric field applied. Φ = workfunction, ε_F = Fermi level.

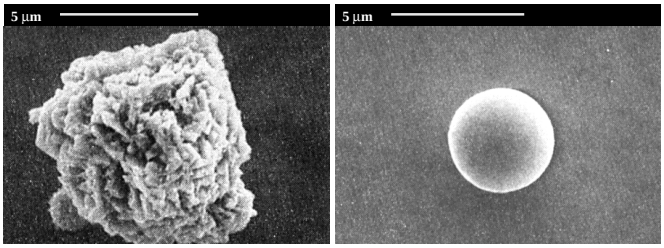

(a) (b)

Fig. 6. DC field-emitting (a) and non-emitting Ni particles (b) [15].

B. Theory of field emission

Although the basic principle of FE is understood, a detailed and quantitative theory of the mechanisms involved is still lacking. The quantum theory of FE was developed by Fowler and Nordheim in 1928 for a metal–vacuum interface (Fig. 5) [12]. Ordinarily, electrons are confined to the wall by a potential barrier (Fig. 5(a)). In the presence of an electric field, however, the infinitely wide barrier is deformed into a triangular, finite-thickness barrier, allowing electrons to tunnel through (Fig. 5(b)). Image-charge effects serve to lower and round the barrier tip.

The theoretical tunneling current density j_{FN} increases exponentially with applied electric field E and is given by

$$j_{\mathrm{FN}} = c_1 E^2 \exp\left(\frac{c_2}{E}\right), \tag{1}$$

where c_1 and c_2 are constants. FE currents observed in cavities follow the same relation, provided one makes the substitution $E \rightarrow \beta_{\mathrm{FN}} E$ for all occurrences of E in (1) [13]. It is, as if the electric field is augmented by a *field-enhancement factor* β_{FN}. β_{FN} values in the range $50 < \beta_{\mathrm{FN}} < 1000$ have been observed [14].

1) Geometric field enhancement: Initially, sharp "whiskers" were thought to be responsible for the field enhancement. Indeed, most FE sites found in DC gaps are jagged, conducting particles (e.g., Fig. 6(a)). Smooth particles, as in Fig. 6(b), do not emit [15]. Similarly, FE in RF cavities occurs exclusively from small particles like the stainless-steel particle in Fig. 7. In fact, studies have shown that the emission characteristics of DC emitters are unchanged when tested in RF fields [16].

However, the field-enhancement factors calculated for simple structures are typically only $\beta_{\mathrm{FN}} \leq 10$ [15], [17].

Structures with moderate aspect ratios can attain $\beta_{\mathrm{FN}} > 10$ if a small projection is present on the tip of a larger one (see Fig. 8). According to this "tip-on-tip" model, the β_{FN} values of each structure roughly multiply to give the overall enhancement factor [15]. Particulate emitters can thereby achieve $\beta_{\mathrm{FN}} \approx 100$.

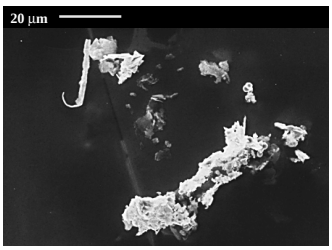

Fig. 7. Stainless-steel emitter found in a 1.5-GHz cavity.

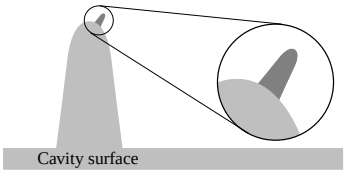

Fig. 8. Schematic of the tip-on-tip model.

Sensitive thermometry demonstrated that the motion of particles in the electric field can lead to the observed activation of FE [8]. One example is shown in Fig. 9(a). It's arrival at the FE site was accompanied by a slight increase in the recorded low-field-temperature signal (Fig. 9(b)).

Similarly, the FE deactivation by particle departure has been observed. If the field is strong enough, particles are "sucked" off the surface [18]. However, as discussed later, other mechanisms also result in the deactivation of FE.

2) Other field-enhancement mechanisms: Many observations remain inconsistent with the tip-on-tip model of FE. For example, in some cases the activation of FE can be precipitated by administering or redistributing gases (e.g., oxygen) in the cavity [8], [11]. Subsequent cycling to room temperature may deactivate the emitters again, only to be reactivated by further admission of gases.

Furthermore, FE can be deactivated by a vacuum bake to ≈ 1000 °C [19], [20]. One might believe that geometric defects become less acute due to the heat treatment. However, subsequent heating to 200–600 °C activates new emitters, thereby ruling out that hypothesis. Instead, the interface between the emitting particles and the substrate may play an important role in governing FE.

In view of such observations, many qualitative, and perhaps somewhat speculative, models for FE enhancement have been developed. They chiefly rely on the fact that contaminants/defects on the RF surface affect the elec-

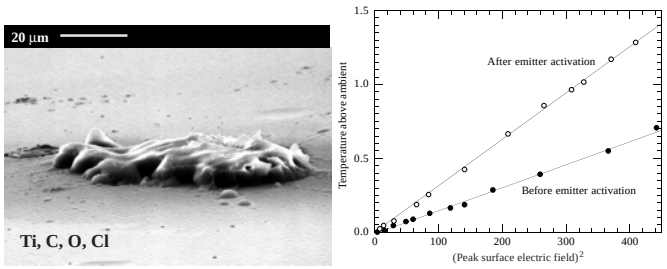

(a) (b)

Fig. 9. (a) FE site that activated by particle motion. The particle melted due to the subsequent FE activity. (b) Increase in the temperature signal at the FE site due to the arrival of the particle.

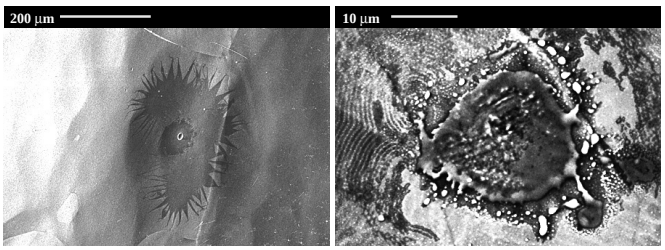

(a) (b)

Fig. 10. (a) Low-magnification micrograph of an RF processed field emitter in a 3-GHz cavity. (b) High-magnification micrograph of an RF processed indium emitter found in a 1.5-GHz cavity.

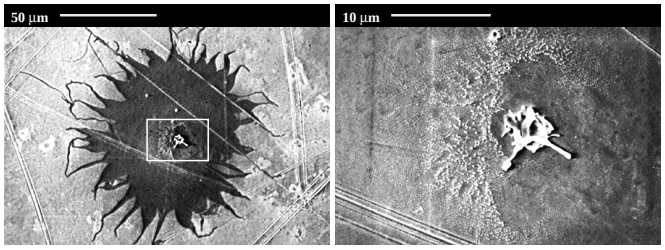

(a) (b)

Fig. 11. Exploded emitter in a 5.8-GHz "mushroom" cavity. (a) Low-magnification picture, (b) magnified view of the framed region.

tronic band structure of the system. Among these theories are the metal–insulator–vacuum (MIV) model [21], the metal–insulator–metal (MIM) model [21], and the resonant tunneling model [22].

It now is believed that FE enhancement is due to a combination of geometric field enhancement and effects involving adsorbates or the interface.

C. Avoiding field emission

1) Cleanliness: Much effort has been expended to reduce FE in RF cavities. Of paramount importance is cleanliness throughout the cavity preparation stages. All cleaning and mounting is carried out in clean rooms with high-purity solvents/water. Prior to assembly, cavities are chemically etched or electropolished to remove 10–100 μm of surface material [23]. Other procedures, such as high-pressure rinsing [24] and heat treatment [25] also reduce contaminants or at least deactivate them.

2) RF processing: Despite all precautions, some particulate contamination is unavoidable. Vacuum accidents and dust migration in accelerators are also likely, so that in situ "cleaning" techniques are needed for efficient operation. One successful method is *high-power processing*, whereby the cavity is pulsed with high power (up to 1 MW for as long as 1 ms) [7]. Often, emitters process. Such events may also occur in continuous wave (cw), low-power operation.

3) RF-processing mechanism: Some cases of RF processing, undoubtedly, are due to the departure of particles mentioned earlier. Frequently, though, processing proceeds by exploding the emitter [26]. Examples are shown in Fig. 10. Low-power (cw) experiments with 5.8-GHz mushroom cavities revealed similar sites (see Fig. 11) [9].

Molten craters and molten debris are found at the center of these sites, surrounded by a larger, dark region called a "starburst."

Starbursts are a common feature of many RF-processed emitters. They are created around DC emitters as well [9], [18]. It is believed that an extended plasma, produced by a discharge during the explosion of the emitter, removes surface adsorbates, thereby creating a "dark" area of reduced secondary-electron-emission coefficient [9], [27].

Initially it was assumed in the SC RF community that the Joule losses of the high-field FE current melt and explode any particles originally at the center of the starburst (see, for example, [7], [9]). The starburst is created as a *result* of the explosion.

In fact, calculations show that the Joule heating is insufficient to create molten structures like those in Fig. 11(b). At best, a region 1 μm across can be melted by this mechanism [8], [28]. Instead, numerical simulations, coupled with thermometry and microscopy, now support the emerging view that other mechanisms are responsible for melting the emitter [8], [29].

In particular, the production of a plasma near the emitter is critical to melting the entire FE site. Initially, on a sub-μsec time scale, submicron tips on the particle emit and are melted by the FE current. Neutral gas desorbs and evolves from these areas due to the sudden deposition of heat. The gas then is ionized by the FE current within 1 μm of the RF surface. The heavy ions linger in the vicinity of the emitter over many RF cycles. Provided the ionization rate (i.e., the emitted current) is high enough, a dense plasma forms and triggers a chain of events leading to the explosion of the emitter: Ions bombard the emitter which again increases the gas evolution and power deposition. The ions also neutralize the FE current, that otherwise can be limited by space-charge effects [30]. Most importantly, the plasma creates an electric field at the RF surface that can attain GV/m levels so that the entire particle begins to emit, even areas for which $\beta_{\mathrm{FN}} < 10$. All these mechanisms provide positive feedback leading to an avalanche situation on a sub-μsec time scale. The power dissipated in the emitting particle is raised by many orders of magnitude. Hundreds of $\mu\mathrm{m}^2$ of the RF surface melt and an explosion results. Ejected droplets in contact with the plasma also emit and explode, which explains why frequently secondary ("satellite") craters are observed near the main FE site [29].

4) Helium processing and mechanism: If high power is not available, the admission of small amounts of He to the cavity (about 0.1–1 mtorr measured at room temperature), while applying RF power, can also precipitate the extinction of emitters ("helium processing") [13].

Several mechanisms have been proposed to explain He processing. They include the erosion and blunting of FE tips by sputtering [13], an alteration of the surface composition by ion implantation [31], and the desorption of adsorbates by impacting ions [13].

Recent thermometry and microscopy studies demonstrate that a number of different "classes" of He processing exist, some of which may involve the mechanisms cited above [8]. However, in many cases He processing acts in the same manner as RF processing. The appearance of

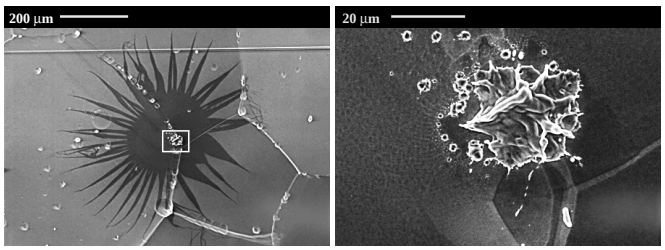

(a) (b)

Fig. 12. Helium processed emitter. (a) Low magn. (b) High magn.

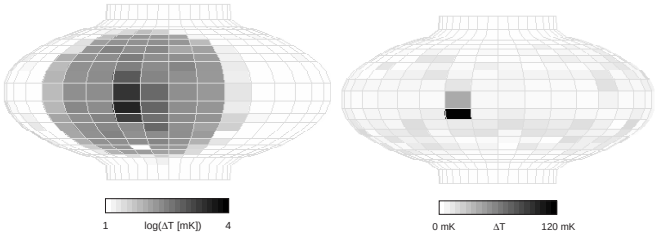

(a) (b)

Fig. 13. (a) A cavity quench during TB. (b) Ohmic heating recorded at the TB center below the TB field.

such processed sites is the same as that of RF processed emitters (Fig. 12) [8]. It is believed, that these emitters did not RF process because the gas-ionization rate was too low, either because the gas density or the emitted current was insufficient (or both). The addition of He then raises the rate of ion production above the processing threshold, be it directly or due to the additional desorption of adsorbates.

IV. Thermal breakdown

A. Diagnosing thermal breakdown

The onset of TB is characterized by a sudden decay of the cavity's stored energy. The time constant for the decay to run its course is on the order of a few milliseconds [32]. Once the stored energy is dissipated, the cavity recovers its original, high-Q_0 state and fills again. TB therefore is self-pulsing. It usually occurs without any precursor such as x rays, or a noticeably declining Q_0. Temperature maps reveal that a large fraction of the cavity quenches during the TB event (Fig. 13(a)). Even below the threshold field, one frequently observes strong, local heating at the center of the TB region, as in Fig. 13(b). Unless TB is caused by bombarding FE electrons, it cannot be processed away! A costly and time consuming cavity disassembly and treatment is then required to remove the source of TB.

B. Thermal breakdown model

TB is triggered by submillimeter, resistive defects on/in the RF surface, primarily in the high-magnetic-field region near the cavity equator. In the steady state, a power $P_{\rm def}$ is dissipated in the defect due to ohmic losses by the RF magnetic field. The power $P_{\rm def}$ has to be conducted by the surrounding Nb to the He bath. If the low thermal

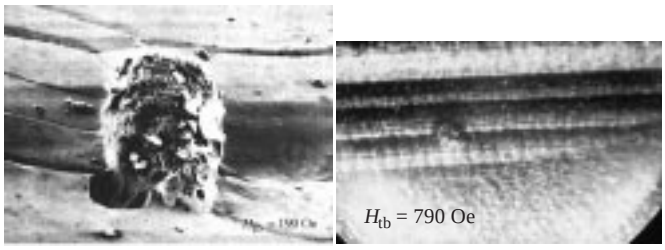

(a) (b)

Fig. 14. Defects observed by thermometry to cause TB. (a) A 360 μm tungsten inclusion in a TIG weld [6]. (b) Possible weld spatter (dia. $\approx$ 1 mm) about 1 cm from an electron-beam weld [8].

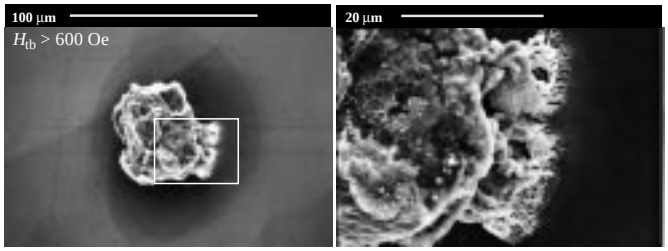

(a) (b)

Fig. 15. A partially melted Cu particle in a 1.5-GHz cavity.

conductivity of SC Nb is not sufficient to thermally stabilize the defect, the SC region surrounding it quenches. The additional resistive area then results in even more power dissipation. This situation is unstable and the normal conducting region expands rapidly (Fig. 13(a)), and dissipating the energy stored in the cavity in a few msec.

A simple analysis of this model yields

$$H_{\rm tb} = \sqrt{\frac{4\kappa_T(T_{\rm c} - T_{\rm b})}{r_{\rm d}R_{\rm d}}}. \qquad (2)$$

for the TB field $H_{\rm tb}$ [1]. Here κ_T is the average thermal conductivity of the Nb, $T_{\rm c}$ is the critical temperature of Nb, $T_{\rm b}$ is the bath temperature, $r_{\rm d}$ is the defect radius, and $R_{\rm d}$ is the surface resistance of the defect. Numerical simulations of TB confirm the general behavior of (2), in particular the $\sqrt{\kappa_T}$ dependence [33], [34].

C. Thermal breakdown defects

Two examples of TB defects are shown in Fig. 14. Occasionally, such defects were introduced during the TIG welding of the cavity. Weld spatter produced during electron-beam (e-beam) welding can also cause TB. Improvements in welding techniques, especially the use of smooth, full-penetration e-beam welds, reduced the occurrence of such defects. TIG welding is no longer used.

Particles introduced during the cavity assembly are also a source of TB. To cause TB, these particles have to be about 1/10–1 mm in size, i.e. they are much larger (and less common) than the smaller field-emitting particles discussed in the previous section. An example is shown in Fig. 15. Interestingly, it appears that the particle is welded to the RF surface. Studies performed at Saclay demonstrate that a loosely adhering particle is not in good thermal contact with the RF surface and little

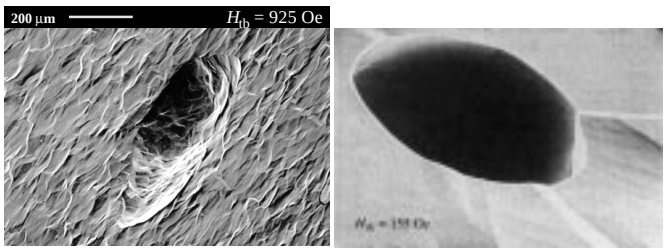

(a) (b)

Fig. 16. Two TB sites. (a) A pit in the RF surface [8]. (b) A 130 μm hole in a TIG weld that quenched at 155 Oe. [6].

ohmic-power dissipation ($\approx$ 10 mW) is required to melt it [35]. However, when the contact areas melt, cooling by the substrate improves and the particle temperature reduces. By this time, the particle may already be attached to the RF surface, making its removal by conventional cleaning techniques difficult.

Nonparticulate defects, such as the pits in Fig. 16, have also been observed to cause TB. In Fig. 16(a) no foreign material was detected by EDX analysis.[2] Regular ohmic losses cannot be responsible for the initiation of TB. Instead, it is speculated that magnetic-field enhancement at the edges of the pits drove the magnetic field above the critical field, thereby precipitating the quench [8].

D. Avoiding thermal breakdown

1) Cleanliness: Akin to FE prevention, cleanliness during cavity production and assembly is critical to avoiding TB, primarily to eliminate particulates and embedded material. The usual steps taken during cavity assembly, such as chemical etching and high-pressure water rinsing are appropriate techniques. An additional requirement is the need for high-quality e-beam welds. Avoidance of the equator welds altogether by hydroforming [36] or spinning [37] cavities, may one day prove useful in minimizing TB.

However, many defects are inclusions in the Nb itself. Such defects cannot always be eliminated by extensive etching or surface cleaning. Quality assurance at the manufacturing stage of the Nb, thus, is paramount.

For example, Nb sheets delivered to DESY are routinely scanned with a special coil that measures eddy currents [38]. Detected defects can be removed by grinding prior to cavity manufacturing.

2) Thermal conductivity: Another approach is to accept the presence of defects but to reduce their ability to initiate TB by increasing the thermal conductivity of Nb. Equation 2 predicts that $H_{\rm tb} \propto \sqrt{\kappa_T}$.

Industry has, in response, raised the purity of as-delivered Nb by a factor of ten over the last decade.[3] The increase was primarily achieved by improving the e-beam-melting techniques used to refine Nb ingots [1].

It is possible to improve the purity by another factor of two to three by heat treatment combined with solid-state gettering. Frequently this is performed as a post-cavity-production step. The process involves coating the cavity with titanium or yttrium (the getter) on both the interior and exterior and heating the cavity to up to 1400 °C in a high vacuum ($\approx 10^{-6}$ torr) for several hours [1], [39]. Interstitial impurities, primarily oxygen, diffuse to the surface and are trapped in the getter. Subsequently, an etch is required to remove the getter and restore the Nb RF surface.

[2] An elemental analysis of the region in Fig. 16(b) is not available.

[3] The thermal conductivity increases roughly linearly with the purity of the Nb.

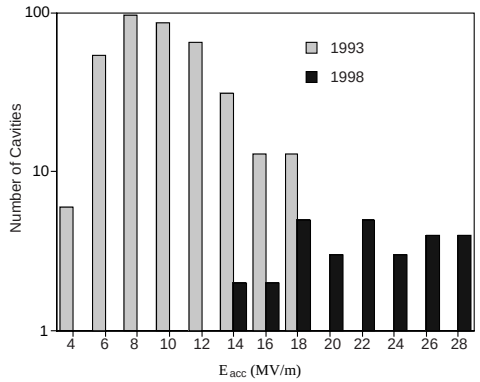

Fig. 17. Improvement in achieved accelerating gradient due to post-purification, high-power processing, and high-pressure rinsing.

V. Summary

FE and TB are the dominant field-limiting mechanisms in superconducting RF cavities. The sources of both FE and TB have been identified. Primarily, micron-size particles are responsible for FE. A combination of geometric field enhancement and other mechanisms, possibly involving the particle–substrate interface, permits electrons to tunnel out of these particles at cavity field levels as low as 10 MV/m. However, a complete understanding of the mechanisms responsible for cavity FE is still lacking.

TB can be caused by inclusions, submillimeter-size particles, and even pits in the RF surface. TB is a quench of the cavity triggered by excessive power dissipation in these defects.

Numerous techniques have been developed to reduce the occurrence of FE and TB in cavities. They include clean-room assembly, high-pressure rinsing, high-power processing, and heat treatment/postpurification. A histogram of achieved gradients as of 1993 and 1998 is presented in Fig. 17 to illustrate the impact of such treatment techniques on the average gradient over the last five years. Although the statistics for 1998 are limited, the improvement of $E_{\rm acc}$ by about $\times 2$ over 1993 is encouraging.

References

[1] H. Padamsee, J. Knobloch, and T. Hays, *RF Superconductivity for Accelerators*, Wiley and Sons, New York, 1998.
[2] H. Piel, In Kuntze [43], pp. 85–118.
[3] G. Müller, In Lengeler [44], pp. 377–408.
[4] R. W. Röth et al., In Proch [45], pp. 599–615.
[5] T. Junquera, A. Le Goff, B. Bonin, H. Safa, and J. Tan, In Sundelin [46], pp. 1014–1019.
[6] H. Padamsee, J. Tückmantel, and W. Weingarten, *IEEE Trans. Magn.*, vol. 19, no. 3, pp. 1308–1311, 1983.
[7] J. H. Graber,, Ph.D. thesis, Cornell University, 1993.

[8] J. Knobloch,, Ph.D. thesis, Cornell University, 1997.
[9] D. Moffat et al., *Part. Accel.*, vol. 40, pp. 85–126, 1992.
[10] R. Noer, *Appl. Phys.*, vol. A 28, pp. 1–24, 1982.
[11] Q. S. Shu et al., *IEEE Trans. Magn.*, vol. 25, pp. 1868–1872, 1989.
[12] R. H. Fowler and L. Nordheim, *Proc. R. Soc. London*, vol. A119, pp. 173–181, 1928.
[13] H. A. Schwettman, J. P. Turneaure, and R. F. Waites, *J. Appl. Phys.*, vol. 45, no. 2, pp. 914–922, 1974.
[14] H. Padamsee, in *The Physics of Particle Accelerators*, M. Month and M. Dienes, Eds., pp. 1403–1482. AIP, 1992, AIP Conf. Proc. 249.
[15] M. Jimenez, R. J. Noer, G. Jouve, J. Jodet, and B. Bonin, *J. Phys. D*, vol. 27, pp. 1038–1045, 1994.
[16] J. Tan, In Bonin [47], pp. 105–117.
[17] H. H. Race, *Gen. Electr. Rev*, vol. 43, no. 9, pp. 365–369, 1940.
[18] R. J. Noer, In Sundelin [46], pp. 236–251.
[19] P. Niedermann,, Ph.D. thesis, University of Geneva, 1986.
[20] E. Mahner, *Part. Accel.*, vol. 46, pp. 67–82, 1994.
[21] N. S. Xu, in *High Voltage Vacuum Insulation*, R. V. Latham, Ed., pp. 115–164. Academic Press, London, 1995.
[22] C. B. Duke and M. E. Alferieff, *J. Chem. Phys.*, vol. 46, pp. 923–937, 1967.
[23] P. Kneisel, In Kuntze [43], pp. 27–40.
[24] P. Kneisel, B. Lewis, and L. Turlington, In Sundelin [46], pp. 628–636.
[25] H. Padamsee et al., in *Proc. 1988 Lin. Accel. Conf.*, Newport News, VA, 1988.
[26] J. Graber et al., *Nucl. Instrum. Methods Phys. Res.*, vol. A 350, pp. 582–594, 1994.
[27] T. Hays et al., In Sundelin [46], pp. 750–762.
[28] J. Knobloch and H. Padamsee, *Part. Accel.*, vol. 53, pp. 53–76, 1996.
[29] J. Knobloch and H. Padamsee, *Part. Accel.*, in press.
[30] P. A. Chatterton, *Proc. Phys. Soc. London*, vol. 88, pp. 231–245, 1966.
[31] S. Bajic and R. Latham, *J. Phys. D*, vol. 21, pp. 943–950, 1988.
[32] M. Pekeler,, Ph.D. thesis, Deutsches Electronen-Synchrotron (DESY), 1996.
[33] H. Padamsee, *IEEE Trans. Magn.*, vol. 19, no. 3, pp. 1322–1325, 1983.
[34] G. Müller, In Shepard [48], pp. 331–358.
[35] J. Tan, H. Safa, and B. Bonin, In Bonin [47], pp. 369–372.
[36] C. Hauviller, in *Proc. 1989 Part. Accel. Conf.*, 1989, p. 485.
[37] V. Palmieri et al., in *Proc. 4th European Part. Accel. Conf*, V. Suller, Ed., 1994, p. 2212.
[38] W. Singer et al., in *Proc. 8th Workshop on RF Supercond.*, Padua, Italy, 1997.
[39] H. Padamsee, *IEEE Trans. Magn.*, vol. 21, no. 2, pp. 1007–1010, 1985.
[40] C. Antoine et al., *J. Appl. Phys.*, vol. 81, no. 4, pp. 1677–1682, 1997.
[41] H. Safa, D. Moffat, F. Kœchlin, E. Jacques, and Y. Boudigou, In Bonin [47], pp. 649–652.
[42] G. Orlandi, C. Bienvenuti, S. Calatroni, and F. Scalambrin, In Sundelin [46], pp. 718–729.
[43] M. Kuntze, Ed., *Proc. Workshop RF Supercond.*, Karlsruhe, Germany, 1980.
[44] H. Lengeler, Ed., *Proc. 2nd Workshop on RF Supercond.*, CERN, Geneva, Switzerland, 1984.
[45] D. Proch, Ed., *Proc. 5th Workshop on RF Supercond.*, Hamburg, Germany, 1991.
[46] R. M. Sundelin, Ed., *Proc. 6th Workshop on RF Supercond.*, Newport News, Virginia, 1993.
[47] B. Bonin, Ed., *Proc. 7th Workshop on RF Supercond.*, Gif-sur-Yvette, France, 1995.
[48] K. W. Shepard, Ed., *Proc. 3rd Workshop on RF Supercond.*, Argonne, Illinois, 1988.